

PREDICTION OF THE PERFORMANCE OF VORTEX-CONTROLLED
DIFFUSER VIA FINITE DIFFERENCE TECHNIQUE

By

ENUMA DICKSON OZOKWELU

School of Chemical Engineering

Oklahoma State University

Stillwater, Oklahoma

Submitted to the Faculty of the Graduate College
of the Oklahoma State University
in partial fulfillment of the requirements
for the Qualifying Examination for the
Degree of
DOCTOR OF PHILOSOPHY
September, 1980

TABLE OF CONTENTS

Chapter	Page
SUMMARY	1
I. INTRODUCTION	4
II. GOVERNING EQUATIONS	8
III. METHOD OF SOLUTION	13
IV. RESULTS AND DISCUSSION OF RESULTS	18
V. CONCLUSIONS AND RECOMMENDATIONS	26
REFERENCES	27
APPENDIX A: THE PROGRAM-SOLA	28
APPENDIX B: BASIC INPUT PARAMETERS FOR THE SOLA PROGRAM	33
APPENDIX C: SAMPLE PROBLEM: VISCOUS FLOW IN A CAVITY	35
APPENDIX D: COPY OF ORIGINAL PROPOSAL	36
APPENDIX E: RESULTS FROM REFERENCES 2 & 1	BEHIND

LIST OF FIGURES

Figure	Page
1. Vortex-Controlled Diffuser (VCD) Geometry	7
2. Flow Mechanism of Vortex Control	7
3. General Mesh Arrangement	9
4. Arrangement of Finite Difference Variables in a Typical Cell	9
5. Problem Schematic	14
6. VCD Velocity Field at Steady State ($t=2.0$ sec) and for 1% Bleed	20
7. VCD Velocity Field at Steady State ($t=2.0$ sec) and for 0% Bleed	21
8. VCD Performance I: Effectiveness Versus Secondary Duct Length for Different Bleed Quantities	22
9. Predicted Coefficient of Static Pressure Rise, C_p for Three Different Inlet Velocity Profiles and Flow Distortions	23
10. VCD Performance II: Effectiveness Versus Area Ratio	24
11. VCD Performance III: Effectiveness Versus Radial Gap	25

"PREDICTION OF THE PERFORMANCE OF VORTEX-CONTROLLED
DIFFUSER VIA FINITE DIFFERENCE TECHNIQUE"

By

Enuma Dickson Ozokwelu

SUMMARY

Scope and Method of Study: Studies in various applications of the vortex-controlled diffuser (VCD) have been done by a few researchers during the last five years because of its obvious advantages over the existing gas turbine engine diffusers. Unfortunately, "Analytical means to predict performance with sufficient accuracy were not available for VCD performance assessment," according to reference 2. Thus in the most recent studies at the DDA (Detroit Diesel Allison, Division of General Motors) it was necessary to experimentally obtain the VCD component parametric performance, for use in the design of the VCD for the combustion system performance evaluation. The work being reported here was aimed at obtaining the VCD component parametric performance theoretically through the use of the 'SOLA' program which is one of the recent computer packages available for solving 2-D incompressible fluid flow problems. The 'SOLA' program employs the finite difference technique to solve the Navier-Stokes equations for incompressible fluid flow in 2-D plane or axisymmetric co-ordinates.

One major reason for choosing SOLA program is its applicability to solving useful and difficult problems, despite its simplicity.

Findings and Conclusions: Vectorial plots of u and v velocity fields for one half of the diffuser (symmetry assumed) revealed that the program successfully predicted the main flow characteristics in accordance with discussions in references 1 and 2: presence of vortex in the vortex chamber; presence of Coanda bubble (Recirculation) at the back of the chamber; and evidence of increase in energy of the flow stream down the secondary duct as a result of the turbulent shear action between adjacent flow streams, brought about by the presence of the vortex. The VCD performance increased with Bleed quantity as well as secondary duct length, but stayed fairly constant after $L/H \approx 0.9$, where L/H is the ratio of length to diameter of the secondary duct length. The performance curves obtained were very similar to the ones in reference 2. A plot of coefficient of ideal diffuser static pressure rise, C_p versus area ratios for different inlet velocity profiles and distortions, was very similar to the one in reference 1. C_p remained unchanged after area ratio of about 3, but increased with inlet distortion for area ratio less than or equal to 3. Thus increased inlet distortion lowered diffuser performance. This seemed to explain why most previous experimenters worked within area ratios not greater than 3. The optimum radial gap was found to be 25 and zero (no gap) percent of the vortex chamber diameter for the annular and tubular diffusers respectively. The effects of secondary duct length, bleed-off quantity, VCD area ratio and VCD inlet flow distortion were similar

for both annular and tubular diffusers. Considering the above findings, the use of SOLA program appears to be the most formidable approach to use in future to estimate VCD component parametric performance, before embarking on any preliminary design.

I

INTRODUCTION

The vortex-controlled diffuser (VCD) employs bleed off at the throat of the diffuser to accomplish low pressure loss diffusion in a short length. Figure 1 borrowed from reference 2 illustrates the simplest form of VCD geometry. The flow diffuses from a primary duct into a suddenly expanded secondary duct. The vortex formed by the presence of the vortex fence introduces a turbulent shear action between adjacent flow streams resulting in an increase of energy of the flow stream down the secondary duct (see Fig. 2). The VCD flow mechanism is very well explained in reference 1.

Studies in various applications of VCD started only about five years ago with the extensive work at the Cranfield Institute of Technology, England. R. C. Adkins (1) et al, working with both tubular and annular diffuser models recommended that the new concept be used to replace existing gas turbine engine diffusers. His results showed that pressure recoveries in excess of eighty percent may be recovered over wide range of area-ratios, with diffuser lengths of about only one-third that required by current design techniques. Only about five percent bleed off of the main air flow from the diffuser throat is required and this bleed off can be used for turbine cooling purposes. Adkins et al (3) showed that the VCD cannot only be used as a precombustor diffuser, but also can be slightly modified for use in

control of exhaust gas emissions from a gas turbine engine. Following the extensive laboratory scale studies at Cranfield, the aerodynamic performance of the VCD as applied to a realistic gas turbine combustor flow path with realistic gas-turbine-diffuser inlet conditions, was studied at DDA (Detroit Diesel Allison, Division of General Motors) under AFAPL (Air Force Aero Propulsion Laboratory) sponsorship. The results proved that the VCD is applicable to gas turbine combustion systems and offers significant diffuser pressure loss reduction. The first phase of the DDA program involved experimentally obtaining the VCD component parametric performance, for use in the design of the VCD for the combustion system performance evaluation. This was necessary because, "Analytical means to predict performance with sufficient accuracy were not available for VCD performance assessment," according to reference 2.

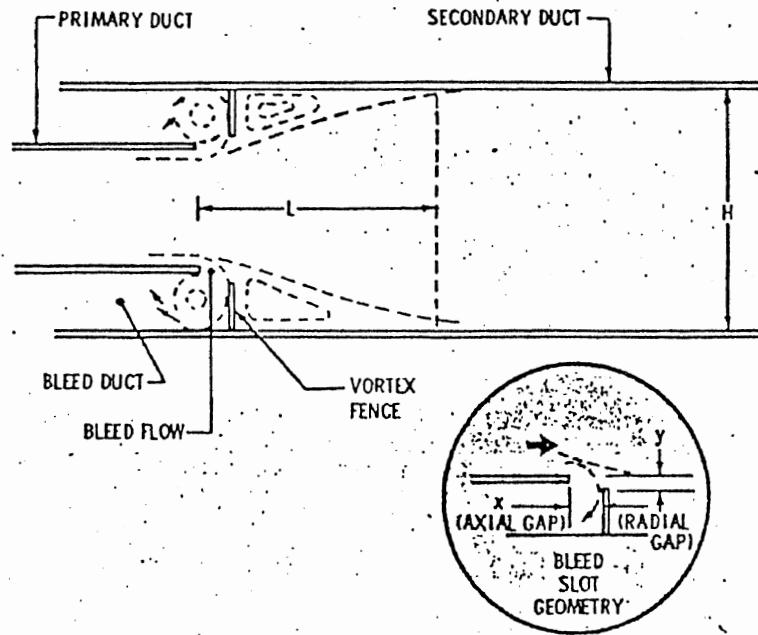
Therefore, the objective here was to use finite difference technique to predict the VCD component parametric performance. This approach appeared to be more economical both money and timewise when compared with the experimental approach at the DDA.

According to White (5), numerical techniques have proved to be the best way to obtain solutions for a number of fluid flow problems that do not have analytical solutions, more especially with the advent of large-scale digital computers. The basic equations solved here were the equation of continuity and the two Navier-stokes equations of motion, in both cartesian and cylindrical (axisymmetric) co-ordinates. The solution set in three dependent variables, pressure, horizontal and vertical velocities (P,U,V) of these equations were used to compute the

VCD component parametric performance. The VCD performance depends on several variables namely:

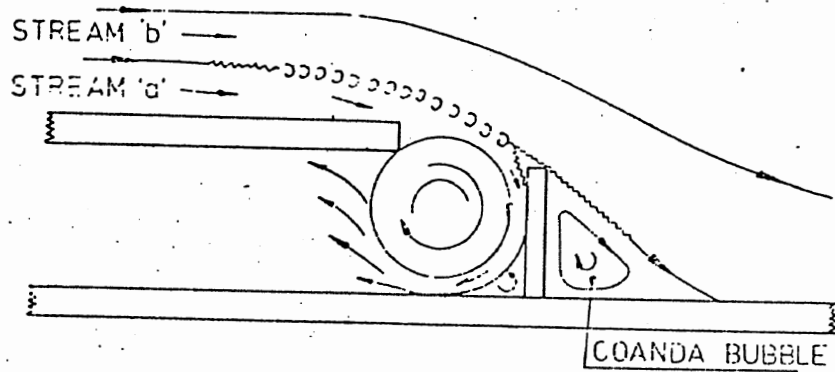
- * Secondary duct length
- * Bleed-off quantity
- * VCD area ratio (A_R)
- * VCD inlet flow distortion
- * Bleed slot radial gaps

In the final analysis, this work was expected to come up with how the VCD performance is affected by changes in the above variables and where possible, the optimum design variables.



VORTEX-CONTROLLED DIFFUSER (VCD) GEOMETRY

FIG. 1



FLOW MECHANISM OF VORTEX CONTROL

FIG. 2

II

GOVERNING EQUATIONS

The equations solved are the equation of continuity:

$$\frac{\partial u}{\partial x} + \frac{\partial v}{\partial y} + \xi \frac{u}{x} = 0 \quad (1)$$

and the two equations of motion:

$$\begin{aligned} \frac{\partial u}{\partial t} + \frac{\partial u^2}{\partial x} + \frac{\partial uv}{\partial y} + \xi \frac{u^2}{x} &= \frac{-\partial p}{\partial x} + g_x + \\ v \left\{ \frac{\partial^2 u}{\partial x^2} + \frac{\partial^2 y}{\partial y^2} + \xi \left(\frac{1}{x} \frac{\partial y}{\partial x} - \frac{y}{x^2} \right) \right\} & \end{aligned} \quad (2a)$$

$$\begin{aligned} \frac{\partial v}{\partial t} + \frac{\partial uv}{\partial x} + \frac{\partial v^2}{\partial y} + \xi \frac{uv}{x} &= \frac{-\partial p}{\partial y} + g_y + \\ v \left\{ \frac{\partial^2 v}{\partial x^2} + \frac{\partial^2 v}{\partial y^2} + \frac{\xi}{x} \frac{\partial v}{\partial x} \right\} & \end{aligned} \quad (2b)$$

The above equations are written in terms of cartesian co-ordinates, (x,y). For cylindrical (axisymmetric) co-ordinates, x, is the radial co-ordinate (r), while y is the axial co-ordinate (z). $\xi = 0$ corresponds to plane geometry, while $\xi = 1$ corresponds to cylindrical geometry. The velocity components u,v are in x and y directions, respectively. P is the ratio of pressure to density, while ν is the kinematic viscosity.

II.A Finite Difference Application

Figure 3 illustrates the finite difference mesh used for numerically solving the equations (1), (2a) and (2b). It consists of cells of

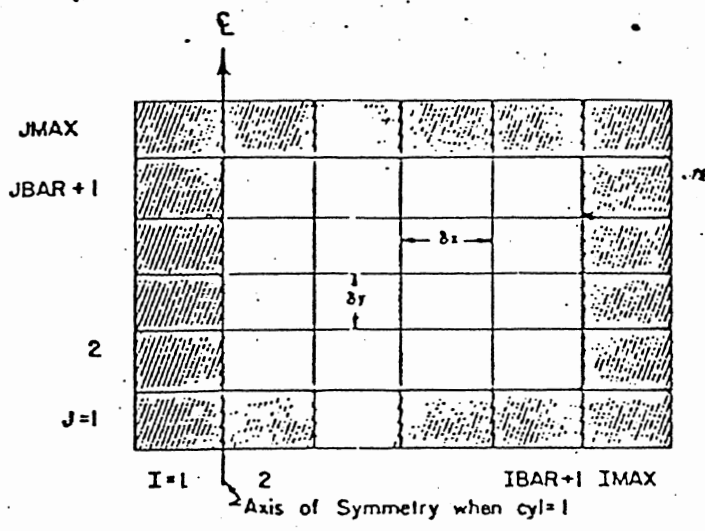


Fig. 3
 General mesh arrangement. Fictitious boundary cells are shaded.

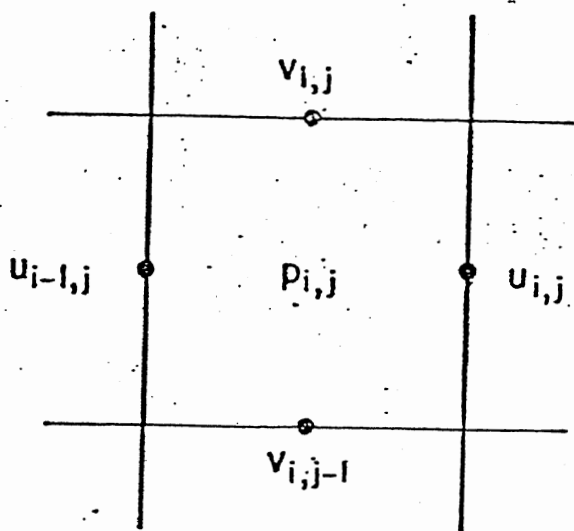


Fig. 4
 Arrangement of finite difference variables in a typical cell.

width x and height y . The fluid is contained in $IBAR \times JBAR$ cells, surrounded by fictitious boundary cells such that the complete mesh has $(IMAX)(JMAX)$ cells where $IMAX = IBAR + 2$ and $JMAX = JBAR + 2$. Figure (2) illustrates the p - u - v locations in each cell, with u and v at the middle of vertical and horizontal sides, respectively, and the pressure at the center.

The finite difference notation used here is:

P_{ij}^n = pressure at center of cell (i,j) at time level n

u_{ij}^n = x -direction velocity at the middle of right side of cell (i,j) at time level n .

v_{ij}^n = y -direction velocity at middle of top side of cell (i,j) at time level n .

The subscripts denote the cell location while the superscripts denote the time level at which quantities are evaluated such that $t = n\delta t$, where δt is the time increment.

Thus, the difference equation representing the equation of continuity [1] is:

$$\frac{1}{\delta x} \left(u_{i,j}^{n+1} - u_{i-1,j}^{n+1} \right) + \frac{1}{\delta y} \left(v_{i,j}^{n+1} - v_{i,j-1}^{n+1} \right) + \frac{\xi}{2\delta x(i-1.5)} \left(u_{i,j}^{n+1} + u_{i-1,j}^{n+1} \right) = 0 \quad (3)$$

All quantities in the above convective and viscous fluxes are to be evaluated at time $n\delta t$. The coefficient α in these expressions give the required amount of upstream (donor cell) differencing. When α is zero, the different equations reduce to numerically unstable centered equations which require some viscosity ν to remain stable. But when α equals one, the equations reduce to full upstream or donor cell form, which is stable provided the fluid does not cross more than one cell in one time step.

The difference equations approximating the Navier-Stokes equations, Eq. (3), are,

$$\begin{aligned}
 u_{i,j}^{n+1} &= u_{i,j}^n + \delta t \left[\frac{1}{\delta x} (p_{i,j}^n - p_{i+1,j}^n) \right. \\
 &+ g_x - FUX - FUY - FUC + VISX \left. \right] \text{ and} \\
 v_{i,j}^{n+1} &= v_{i,j}^n + \delta t \left[\frac{1}{\delta y} (p_{i,j}^n - p_{i,j+1}^n) \right. \\
 &+ g_y - FVX - FVY - FVC + VISY \left. \right], \quad (4)
 \end{aligned}$$

where the convective and viscous fluxes are defined as

$$\begin{aligned}
 FUX &= \frac{1}{4\delta x} \left[(u_{i,j} + u_{i+1,j})^2 + \alpha |u_{i,j} + u_{i+1,j}| \cdot \right. \\
 &\quad \left. (u_{i,j} - u_{i+1,j}) - (u_{i-1,j} + u_{i,j})^2 \right. \\
 &\quad \left. - \alpha |u_{i-1,j} + u_{i,j}| (u_{i-1,j} - u_{i,j}) \right], \\
 FUY &= \frac{1}{4\delta y} \left[(v_{i,j} + v_{i+1,j}) (u_{i,j} + u_{i,j+1}) \right. \\
 &\quad + \alpha |v_{i,j} + v_{i+1,j}| (u_{i,j} - u_{i,j+1}) \\
 &\quad - (v_{i,j-1} + v_{i+1,j-1}) (u_{i,j-1} + u_{i,j}) \\
 &\quad \left. - \alpha |v_{i,j-1} + v_{i+1,j-1}| (u_{i,j-1} - u_{i,j}) \right], \\
 FUC &= \frac{\xi}{8\delta x(i-1)} \left[(u_{i,j} + u_{i+1,j})^2 + (u_{i-1,j} + u_{i,j})^2 \right. \\
 &\quad + \alpha |u_{i,j} + u_{i+1,j}| (u_{i,j} - u_{i+1,j}) \\
 &\quad \left. + \alpha |u_{i-1,j} + u_{i,j}| (u_{i-1,j} - u_{i,j}) \right], \\
 FVX &= \frac{1}{4\delta x} \left[(u_{i,j} + u_{i,j+1}) (v_{i,j} + v_{i+1,j}) \right. \\
 &\quad + \alpha |u_{i,j} + u_{i,j+1}| (v_{i,j} - v_{i+1,j}) \\
 &\quad - (u_{i-1,j} + u_{i-1,j+1}) (v_{i-1,j} + v_{i,j}) \\
 &\quad \left. - \alpha |u_{i-1,j} + u_{i-1,j+1}| (v_{i-1,j} - v_{i,j}) \right]
 \end{aligned}$$

$$\begin{aligned}
 FVY &= \frac{1}{4\delta y} \left[(v_{i,j} + v_{i,j+1})^2 + \alpha |v_{i,j} + v_{i,j+1}| \cdot \right. \\
 &\quad \left. (v_{i,j} - v_{i,j+1}) - (v_{i,j-1} + v_{i,j})^2 \right. \\
 &\quad \left. - \alpha |v_{i,j-1} + v_{i,j}| (v_{i,j-1} - v_{i,j}) \right], \\
 FVC &= \frac{\xi}{8\delta x(i-1.5)} \left[(u_{i,j} + u_{i,j+1}) (v_{i,j} + v_{i+1,j}) \right. \\
 &\quad + (u_{i-1,j} + u_{i-1,j+1}) (v_{i-1,j} + v_{i,j}) \\
 &\quad + \alpha |u_{i,j} + u_{i,j+1}| (v_{i,j} - v_{i+1,j}) \\
 &\quad \left. + \alpha |u_{i-1,j} + u_{i-1,j+1}| (v_{i-1,j} - v_{i,j}) \right], \\
 VISX &= \nu \left[\frac{1}{\delta x^2} (u_{i+1,j} - 2u_{i,j} + u_{i-1,j}) \right. \\
 &\quad + \frac{1}{\delta y^2} (u_{i,j+1} - 2u_{i,j} + u_{i,j-1}) \\
 &\quad \left. + \frac{\xi}{2\delta x^2(i-1)} (u_{i+1,j} - u_{i-1,j}) - \frac{\xi u_{i,j}}{\delta x^2(i-1)^2} \right]
 \end{aligned}$$

and

$$\begin{aligned}
 VISY &= \nu \left[\frac{1}{\delta x^2} (v_{i+1,j} - 2v_{i,j} + v_{i-1,j}) \right. \\
 &\quad + \frac{1}{\delta y^2} (v_{i,j+1} - 2v_{i,j} + v_{i,j-1}) \\
 &\quad \left. + \frac{\xi}{2\delta x^2(i-1.5)} (v_{i+1,j} - v_{i-1,j}) \right]
 \end{aligned}$$

II.B Numerical Stability

Numerical instability occurs when computed quantities develop large, high frequency oscillations in space, time, or both [6], thereby giving highly inaccurate results. To avoid this, care must be exercised in choosing δx , δy , δt and α . The procedure would be:

- a. Choose the mesh increments δx , δy .
- b. Choose the time increment δt subject to the following two limitations:
 - i. Material cannot move through more than one cell in one time step because the difference equations assume fluxes only between adjacent cells, hence:

$$\delta t < \min \left\{ \frac{\delta x}{|u|}, \frac{\delta y}{|v|} \right\}$$

where the minimum is with respect to every cell in the mesh. Usually δt chosen equals $1/4$ to $1/3$ of the minimum cell transit time.

- ii. When a non-zero value of kinematic viscosity, ν is used, momentum must not diffuse more than approximately one cell in one time step, i.e.,

$$\nu \delta t < \frac{1}{2} \frac{\delta x^2 \delta y^2}{\delta x^2 + \delta y^2}$$

- c. Finally choose α such that:

$$1 \geq \alpha > \max \left\{ \left| \frac{u \delta t}{\delta x} \right|, \left| \frac{v \delta t}{\delta y} \right| \right\}$$

Usually, $\alpha = 1.2$ to 1.5 times of $\max \left\{ \left| \frac{u \delta t}{\delta x} \right|, \left| \frac{v \delta t}{\delta y} \right| \right\}$

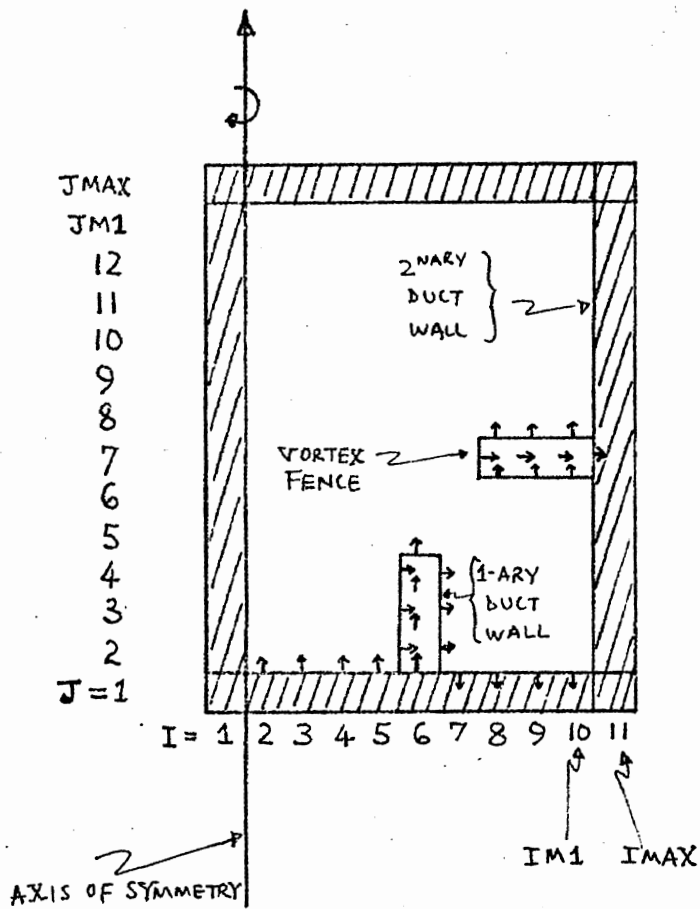
III

METHOD OF SOLUTION

Firstly, the problem was simulated to fit the SOLA algorithm by making a detailed analyzed schematic of the problem. Then the input data were selected, including the boundary conditions. Careful attention was paid to obtaining special boundary conditions from the problem schematic. These parts were then put into their appropriate positions in the program deck and the program run for that particular case. This process was repeated for all the different cases run.

The next four pages contain the problem schematic, input data and special boundary conditions for the various cases studied.

The problem, viscous flow in a cavity, was used as a sample test problem. In other words, it was used to debug the program. To make sure that the program was working well, the sample test problem was run until the results obtained were exactly the same as those obtained by C. W. Hirt et al. (6).



Input Data List

EPSI = 5.0E-03	WL = 1
DELX = 0.2	WR = 1
DELY = 0.4	WT = 3
IBAR = 9	WB = 1
JBAR = 12	DZRO = 1.0
GX = 0.	UI = 0.
GY = 0.	VI = 2.0
CYL = 0.	ALPHA = 0.5
OMG = 1.7	DELT = 0.5
	NU = 2.5E-04

Fig. 5: PROBLEM SCHEMATIC: FLOW IN A VCD

Special Boundary Conditions

Case 1: Effectiveness Versus L/H with % Bleed as Parameter

L = Length of secondary duct

H = Diameter of secondary duct

VI = Average inlet velocity.

(1) L was varied by varying the JBAR in the program.

JBAR = 8, 14, 2

(2) For the primary duct wall

$$U_{i,j} = 0 \text{ for } i = 5, 6 \text{ \& } j = 2, 4$$

$$V_{6,j} = 0 \text{ for } j = 1, 4$$

(3) Inlet & Bleed Velocities

Mean flow rate was generated by defining a constant axial velocity VI across the bottom of the computing mesh and -B% VI across the bottom of the vortex chamber.

$$V_{i,1} = VI \text{ for } i = 2, 5$$

and

$$V_{i,1} = -B * VI \text{ for } i = 7, 10$$

(4) For the Vortex Fence

$$U_{i,7} = 0 \text{ for } i = 7, 10$$

$$V_{i,j} = 0 \text{ for } i = 8, 10 \text{ \& } j = 6, 7$$

(5) Different Bleed rates were simply introduced by varying B from 0 to 12.

Case 2: Effectiveness Versus Area Ratio (A_R) With Inlet Flow Distortion as Parameter.

- (1) Different area ratios were achieved by varying IN

IN \equiv Fluid Column adjacent to the left side of the primary duct wall.

- (2) For the Primary Duct Wall

$$U_{i,j} = 0 \text{ for } i = \text{IN}, \text{IN} + 1 \text{ \& } j = 2, 4$$

$$V_{i,j} = 0 \text{ for } i = \text{IN} + 1 \text{ \& } j = 1, 4$$

- (3) For the Vortex Fence

$$V_{i,7} = 0 \text{ for } i = \text{IN} + 2, 10$$

$$V_{i,j} = 0 \text{ for } i = \text{IN} + 3, 10 \text{ \& } j = 6, 7$$

- (4) Inlet & Bleed Velocities

Distortion was introduced by defining varying axial velocities across the bottom of the computing mesh and $-B \times VI$ across the bottom of the vortex chamber.

$$V_{i,1} = 2.4 \text{ for } i = 2, \text{IN}, 2$$

$$V_{i,1} = 1.6 \text{ for } i = 3, \text{IN}, 2$$

$$V_{i,1} = -B * VI \text{ for } i = \text{IN} + 2, 8$$

Case 3: Effectiveness Versus Radial Gap

Change in radial gap was achieved by simply varying the vortex fence height.

- No Gap : $U_{i,7} = 0$ for $i = 6, 10$; $V_{i,j} = 0$ for $i = 7, 10$ & $j = 6, 7$
- 1 Gap : $U_{i,7} = 0$ for $i = 7, 10$; $V_{i,j} = 0$ for $i = 8, 10$ & $j = 6, 7$
- 2 Gaps : $U_{i,7} = 0$ for $i = 8, 10$; $V_{i,j} = 0$ for $i = 9, 10$ & $j = 6, 7$
- 3 Gaps : $U_{i,7} = 0$ for $i = 9, 10$; $V_{10,j} = 0$ for $j = 6, 7$
- 4 Gaps (no fence) : $U_{10,7} = 0$

IV

RESULTS AND DISCUSSION OF RESULTS

The results obtained were displayed in figures 6 to 11.

(A): Figures 6 and 7 show the vector plot of u and v velocity field for one half of the diffuser (symmetry assumed). This was necessary initially in order to see if the program predicted the main flow characteristics discussed in references 1 and 2, and it did! R1 is the vortex region in the vortex chamber. R2 shows the Coanda Bubble⁽¹⁾ or recirculation zone at the back of the vortex fence. R3 confirmed the increase in energy of the flow stream down the secondary duct as a result of the turbulent shear action between adjacent flow streams, brought about by the presence of the vortex. In fig. 7, fluid flowed into the vortex chamber and completely made a turn-around as expected because of the special boundary condition in the program for zero percent bleed.

(B): The performance curves shown in fig. 8 are very similar to figures 7 & 8 in reference 2. They confirm that (i) the VCD performance increased with secondary duct length but stayed constant after about $L/H \approx 0.9$ (ii) the VCD performance increased with bleed quantity.

(C): The dependency of coefficient of ideal diffuser static pressure rise, C_p on the area ratio for different velocity profiles and

inlet distortions are illustrated in fig. 9. This plot is again similar to fig. 10 in reference 1. Notice that:

(i) C_p decreased with increased area ratios, but remained almost unchanged after area-ratio of about 3.

(ii) For area ratios not more than 3, increased inlet flow distortion increased C_p . But C_p is inversely proportional to diffuser effectiveness which is defined in reference 1 as

$$\xi \equiv \frac{\text{measured static pressure rise}}{C_p (1/2 \rho \bar{V}_1^2)}$$

where ξ is diffuser effectiveness

ρ is fluid density

\bar{V}_1 is average inlet velocity

Consequently, increased inlet distortion would lower diffuser performance for area ratios not more than 3. Fig. 10 confirmed this. This probably offers an explanation why most previous experimenters worked within the limit of $A_R \leq 3$.

(D): Fig. 11 illustrates the effect of radial gaps on VCD performance. The optimum radial gap appeared to zero (no gap at all) for the tubular diffuser and about twenty-five percent of the vortex-chamber diameter for the annular diffuser.

Figures 6, 7 and 8 have similar patterns for both kinds of diffusers. There were slight but very negligible shift in the curves. Figures 9 and 10 are the same for both diffuser types.

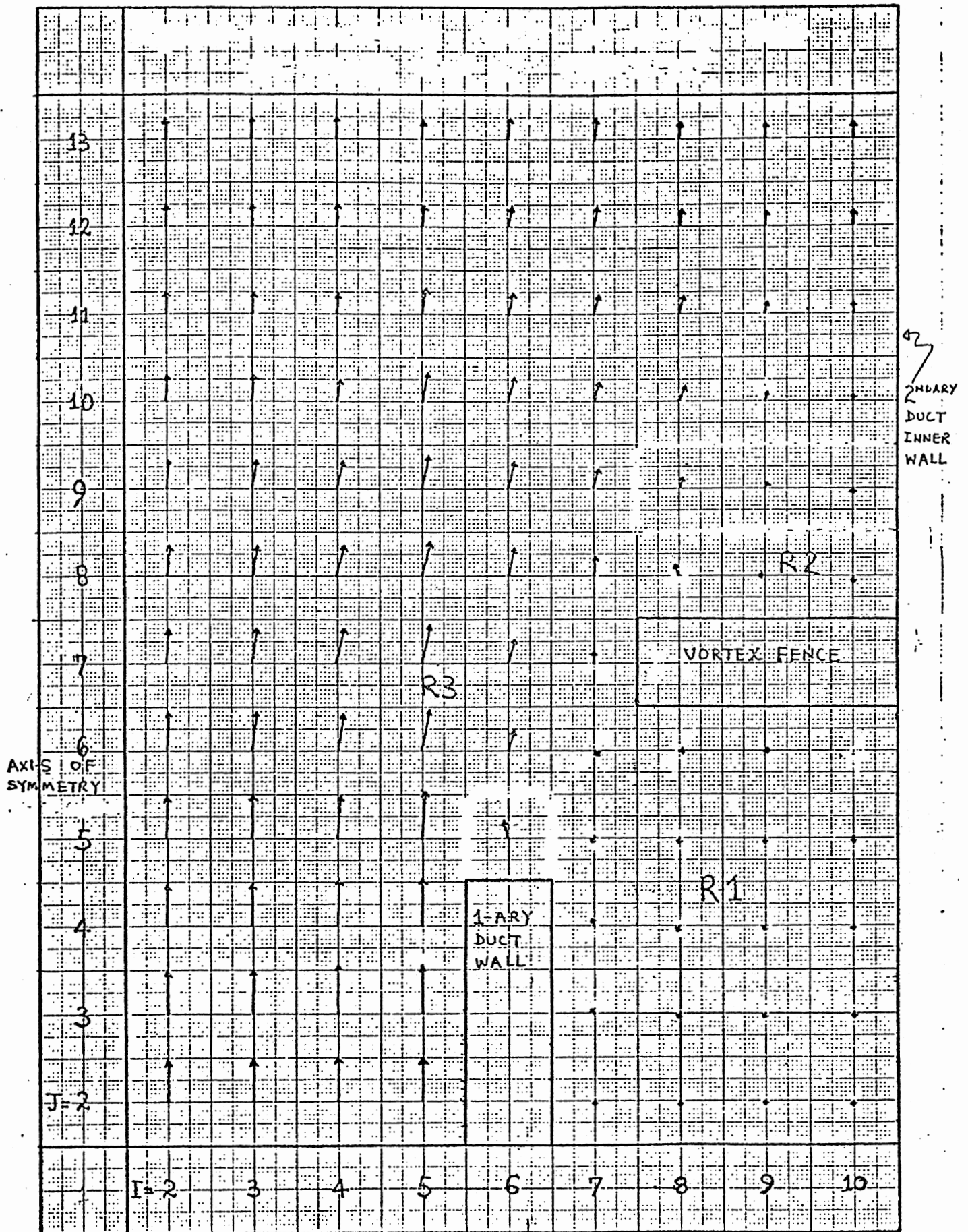


Fig. 6: VCD Velocity Field at Steady State ($t=2.0$ sec) and for 1% Bleed

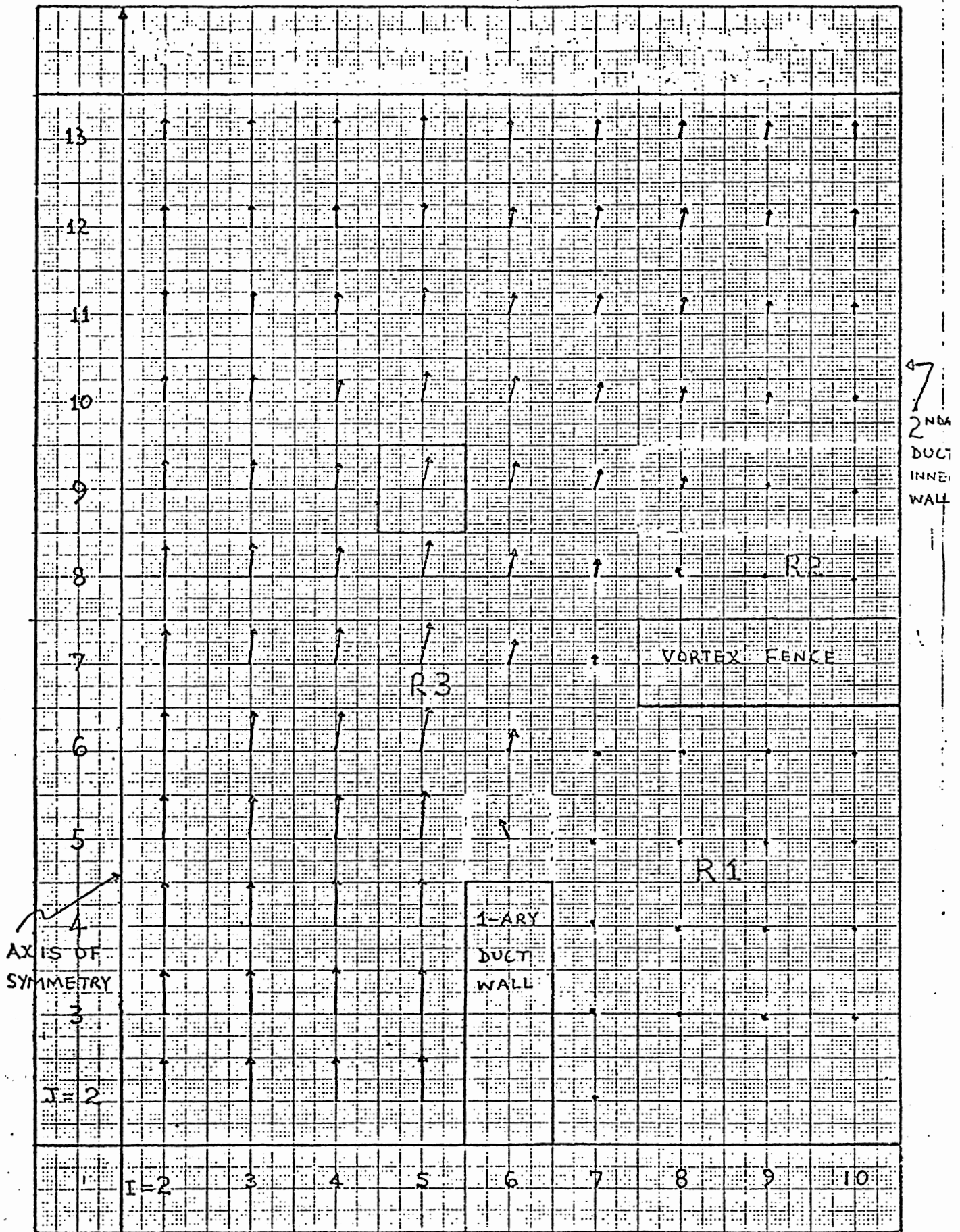


Fig. 7: VCD Velocity Field at Steady State ($t=2.0$ sec) and for 0% Bleed

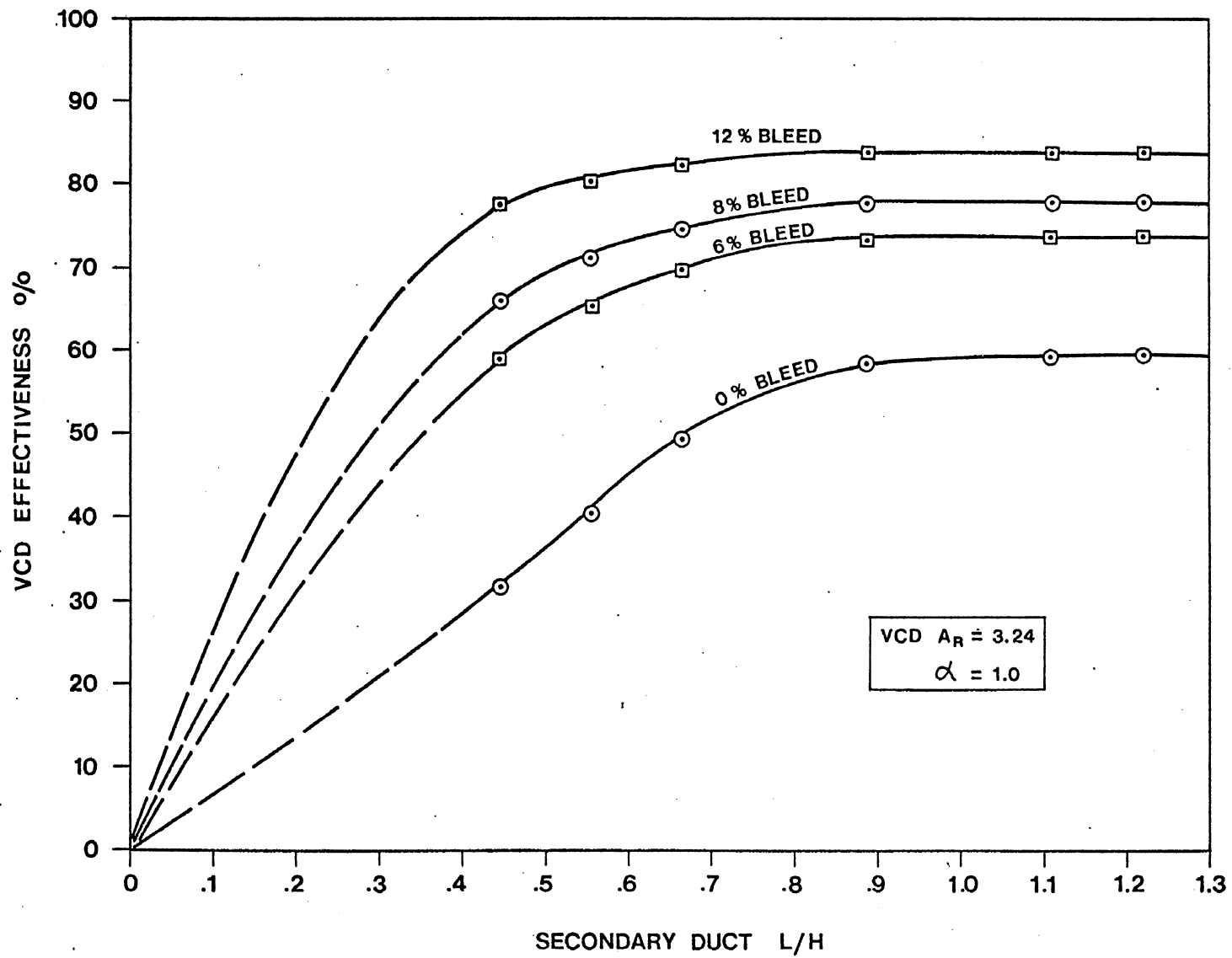


Figure 8. VCD PERFORMANCE I

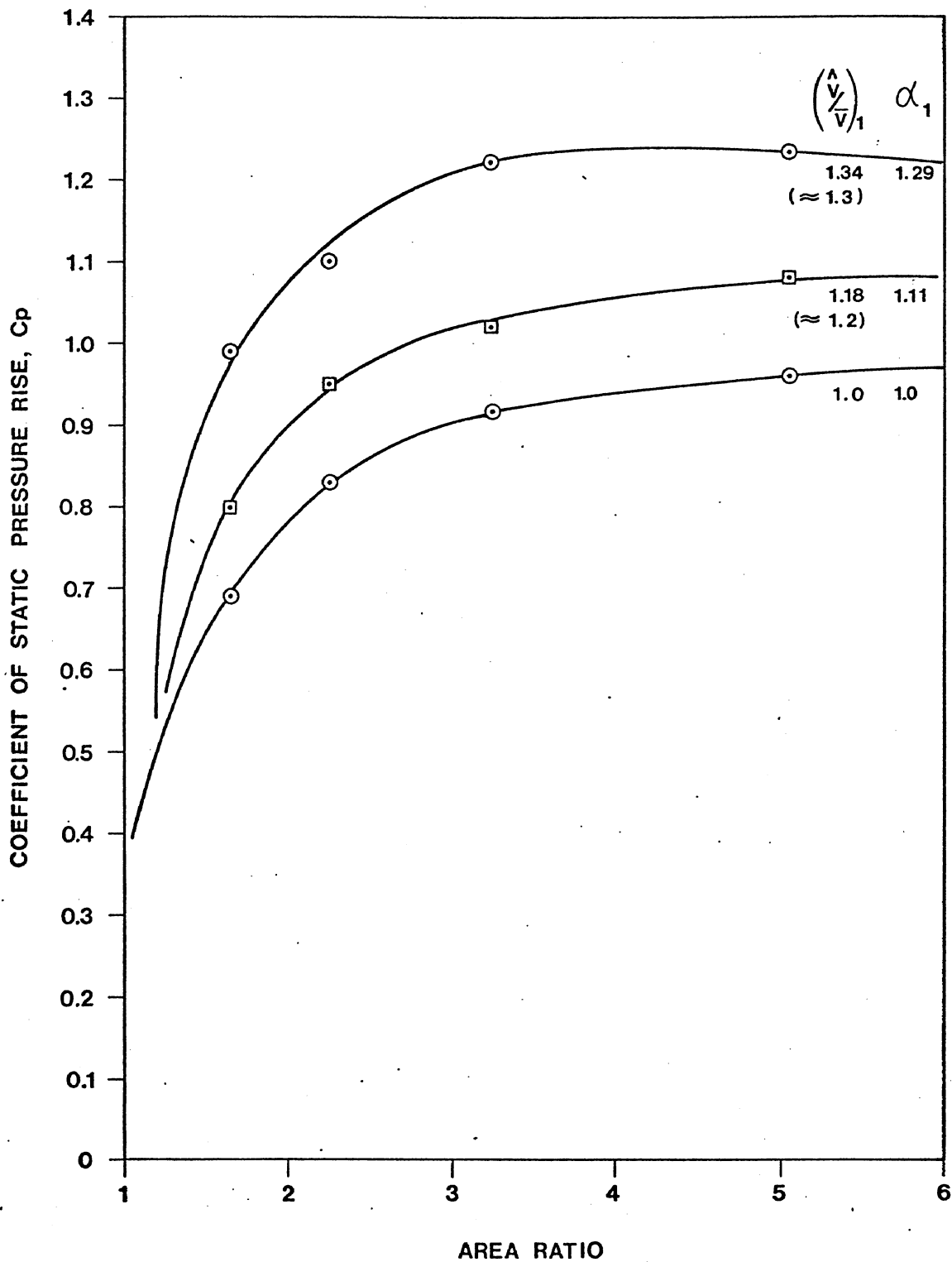


Figure 9. PREDICTED COEFFICIENT OF STATIC PRESSURE RISE, C_p FOR THREE DIFFERENT INLET VELOCITY PROFILES

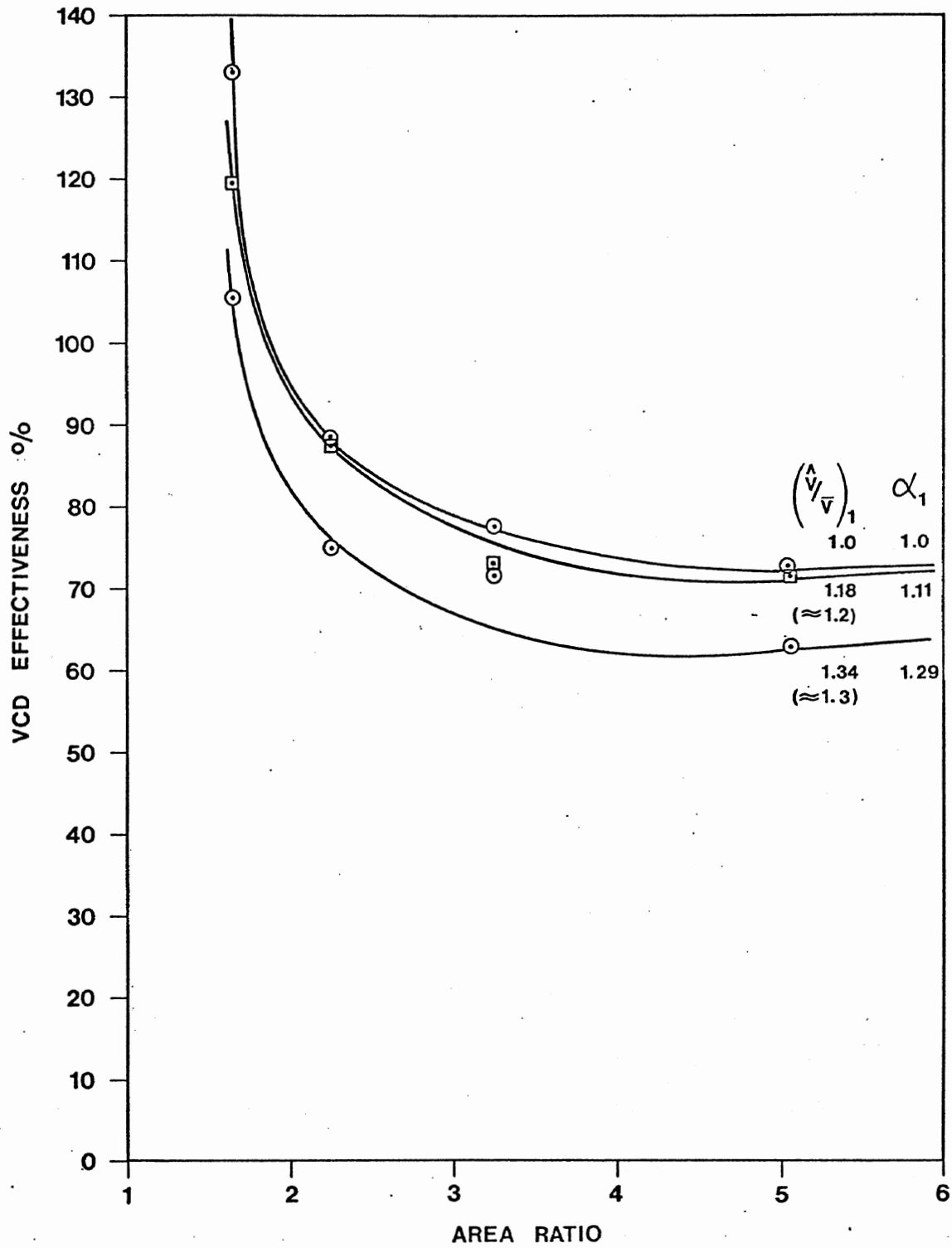


Figure 10. VCD PERFORMANCE II

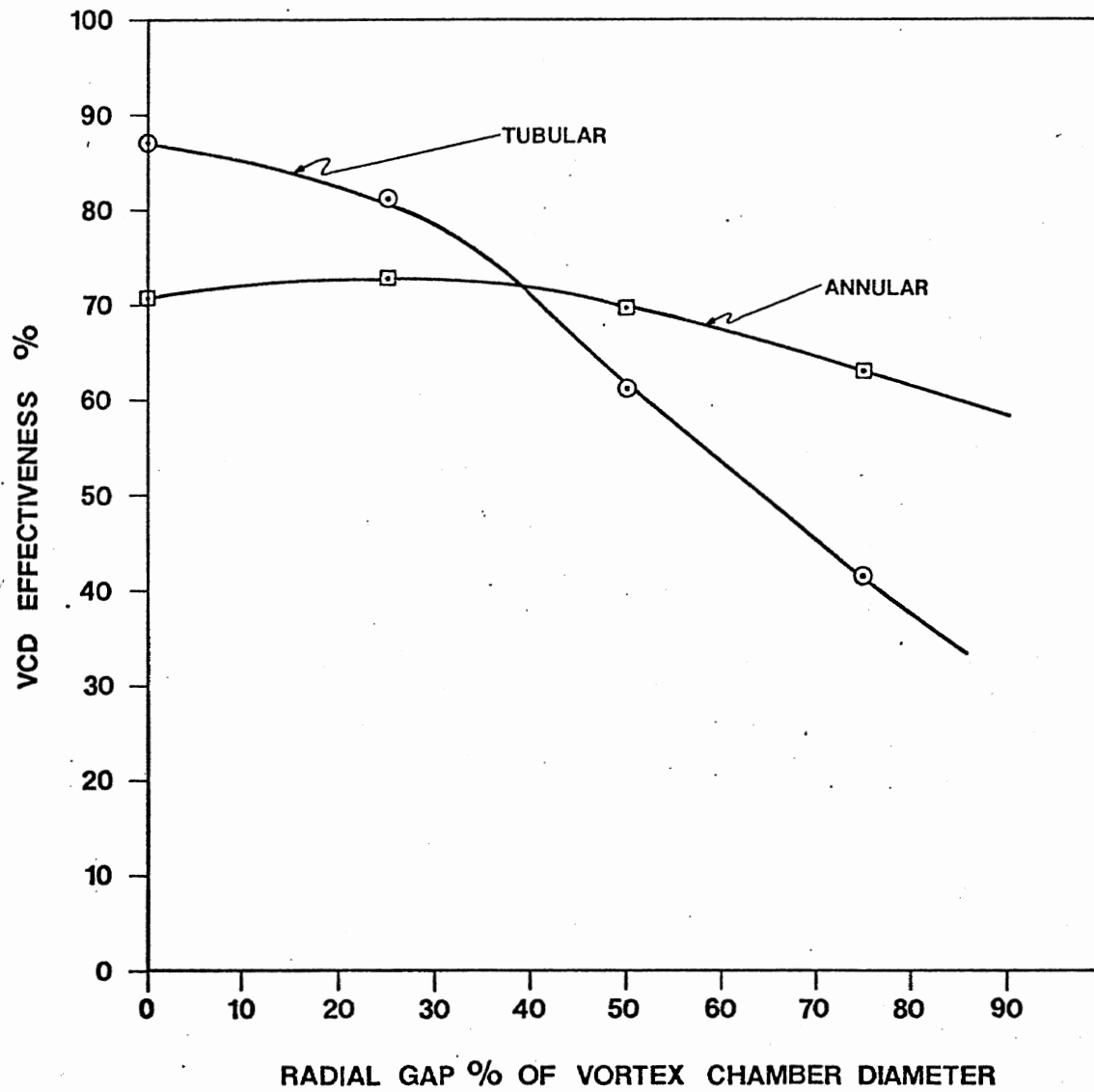


Figure 11: VCD PERFORMANCE III

V

CONCLUSIONS AND RECOMMENDATIONS

The VCD component parametric performance have been obtained via numerical technique: It increased with secondary duct length up to a limit of $L/H \approx 0.9$; increased with bleed quantity; decreased with area ratio up to a limit of $A_R \leq 3$; and decreased with inlet flow distortion. In preliminary design of diffusers, no radial gap is recommended for tubular type while a radial gap of 25 percent of the vortex chamber is recommended for annular diffusers. This method has been proved to be a better way to obtain VCD component parametric performance for initial VCD performance appraisal. Compared with the experimental method used at the DDA program ⁽²⁾, it saves time and money and is therefore highly recommended for use in the future.

REFERENCES

1. Adkins R. C., "A Short Diffuser With Low Pressure Loss," Cranefield Institute of Technology, England, Paper presented at ASME-CSME Fluids Engineering Conference, Quebec, Canada, May 1974.
2. A. J. Verdouw, "Performance of the Vortex-Controlled Diffuser (VCD) in an Annular Combustor Flowpath," Detroit Diesel, Allison, Indianapolis, Indiana.
3. Adkins, R. C., and Elsaflany, A. S., "A Double Acting Variable Geometry Combustor," Contributed by the Gas Turbine Division of the ASME for presentation at the Gas Turbine Conference and Exhibit and Solar Energy Conference, San Diego, California, March 12-15, 1979.
4. Nahavandi, A. N., Holder, G. D. and Borhani, M. A., "Numerical Modelling of Thermal Effects in Turbulent Mixing of Large Flows," Dept. of Chemical Engineering, Columbia Univ., N.Y., The Canadian Journal of Chemical Engineering, Vol. 57, August 1979.
5. Frank M. White, "Viscous Fluid Flow," McGraw Hill Book Company, 1974.
6. Hirt, C. W. et al., "Sola - A Numerical Solution Algorithm for Transient Fluid Flows."

APPENDIX A

THE PROGRAM 'SOLA'

A-1: Program Logic

The logic is centered on solving equation (4) subject to continuity equation (3). Velocities obtained as solutions to (4) usually do not satisfy equation of continuity. This incompressibility constraint is imposed by adjusting the cell pressures. Suppose the left hand side of equation (3) is known as the divergence (div.) of cell D, the objective is to keep adjusting the cell pressures in (4) until D equals zero. A case of negative value for D implies inflow of mass into the cell, hence pressure has to increase to eliminate the inflow. Conversely, a positive value for D would imply outflow of mass from the cell, in which case, pressure has to be reduced to draw the flow back. This way, the divergence of the cell is driven to zero. Unfortunately, adjustment of pressure for one cell affects its neighbors, hence adjustment of cell pressures has to be done iteratively throughout the whole mesh sweeping from left to right and starting from bottom row and working upwards. The pressure change required to drive D to zero is:

$$\delta_p = \frac{-D}{2\delta t \left(\frac{1}{\delta x^2} + \frac{1}{\delta y^2} \right)} \quad (5)$$

and the new cell pressure then becomes:

$$P_{i,j} + P_{i,j} + \delta_p$$

The velocity components at the cell sides then become:

$$\left. \begin{aligned} u_{i,j} &\leftarrow u_{i,j} + \frac{\delta t \delta p}{\delta x} \\ u_{i-1,j} &\leftarrow u_{i-1,j} - \frac{\delta t \delta p}{\delta x} \\ v_{i,j} &\leftarrow v_{i,j} + \frac{\delta t \delta p}{\delta y} \\ v_{i,j-1} &\leftarrow v_{i,j-1} - \frac{\delta t \delta p}{\delta y} \end{aligned} \right\} \quad (6)$$

Usually convergence of the iteration is accelerated by use of over-relaxation parameter ω . A good value for ω is about 1.8 maximum, but it must never be more than 2.

$$\text{NOW BETA} = \omega \left[2\delta t \left(\frac{1}{\delta x^2} + \frac{1}{\delta y^2} \right) \right] \quad (7)$$

Convergence is achieved when $|D/D_0| < \epsilon$ where D_0 is some reference value, usually 1 and ϵ is of the order of 10^{-3} .

Thus a summary of the program logic would be:

1. Compute new guesses for u, v for entire mesh using equation (4) with previous time values of p, u, v in various flux contributions.
2. Adjust u, v iteratively to satisfy equation (3) by making appropriate changes in cell pressure, p .
3. At convergence, p, u, v at advanced time level are obtained and may be used as starting values for next cycle.

Figure 3 is an illustrative flow chart for the program, while the program is listed in Appendix A.

A-2: Input Data and Boundary Conditions

A comprehensive list of input data is described in Appendix B. Of special interest is the simplified way of setting boundary conditions by use of input numbers:

(4) Periodic in X: $U_{1,j} = U_{IBAR,j}$ for all j on the left
 $V_{1,j} = V_{IBAR,j}$

and $U_{1,j} = U_{IBAR,j}$ $V_{2,j} = V_{IBAR + 1, j}$ for all j on the right
 $P_{2,j} = P_{IBAR + 1, j}$ $V_{1,j} = V_{IBAR, j}$

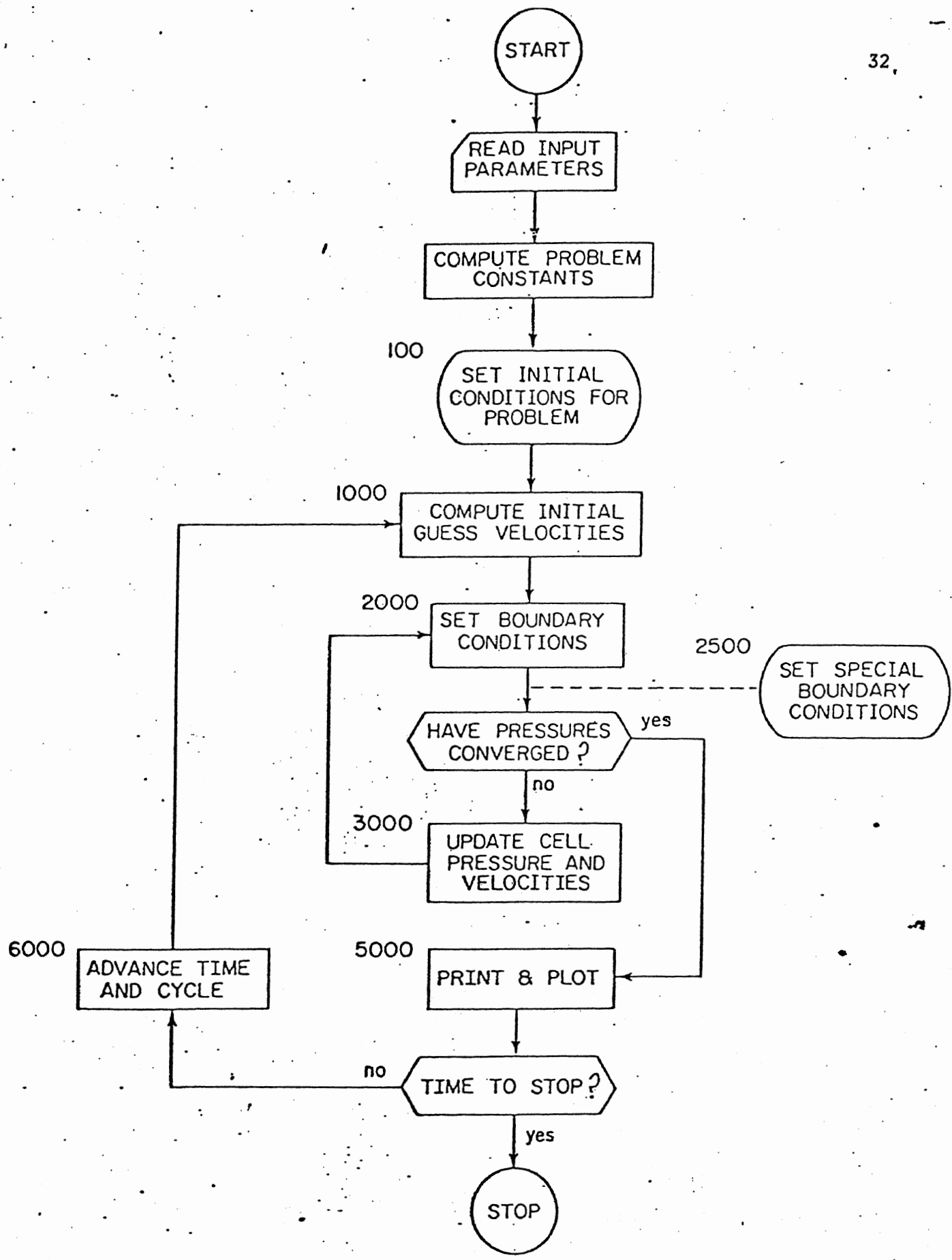


FIGURE 12. Flow Chart for "SOLA" Program

APPENDIX B. BASIC INPUT PARAMETERS FOR THE SOLA PROGRAM

The basic input parameters that must be defined for every problem are as follows:

IBAR = number of cells in the x-direction (excluding boundary cells)

JBAR = number of cells in the y-direction (excluding boundary cells)

DELX = δx = width of cell in x-direction

DELY = δy = height of cell in y-direction

DELT = δt = time increment

NU = ν = coefficient of kinematic viscosity

CYL = ξ = geometry indicator (1.0 for cylindrical coordinates, 0.0 for plane coordinates)

EPSI = ϵ = pressure iteration convergence criterion

DZRO = D_0 scaling factor for convergence test

GX = g_x = body acceleration in positive x-direction

GY = g_y = body acceleration in positive y-direction

UI = x-direction velocity used for initializing mesh and/or setting special boundary conditions

VI = y-direction velocity used for initializing mesh and/or setting special boundary conditions

VELMX = maximum velocity expected in problem, used to scale velocity vector plot

TWFIN = problem time when calculation is to be terminated

CWPRT = number of cycles between long prints output on paper

CWPLT = number of cycles between plots and listings to be output on film

OMG = ω = over-relaxation factor used in pressure iteration

ALPHA = α = controls amount of donor cell fluxing (1.0 for full donor cell differencing and 0.0 for centered differencing.)

WL = indicator for boundary condition to be used along the left side of the mesh (1.0 = rigid free-slip wall, 2.0 = rigid no-slip wall, 3.0 = continuative boundary, and 4.0 = periodic boundary)

WR = indicator for boundary condition along right side of mesh (see WL)

WT = indicator for boundary condition along top of mesh (see WL)

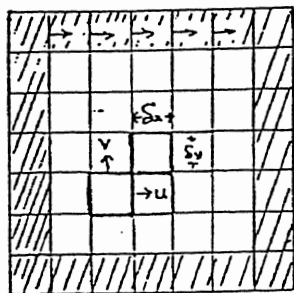
WB = indicator for boundary condition along bottom of mesh (see WL).

The following listing of SOLA is for a CDC-7600 computer at the Los Alamos Scientific Laboratory (LASL). The program, in FORTRAN IV, should be

APPENDIX C: PROBLEM SCHEMATIC AND RESULTS FOR VISCOUS FLOW IN
A CAVITY USED TO DEBUG THE SOLA PROGRAM DECK

INPUT DATA LIST

JMAX = 7
JBAR+1 6
5
4
3
2
J=1



I=1 2 3 4 5 6 7
IBAR+1 ↗
IMAX ↑

EPSI = 5.0 E-03	WL = 2
DELX = 0.2	WR = 2
DELY = 0.2	WT = 2
IBAR = 5	WB = 2
JBAR = 5	DZRO = 1.
GX = 0.	UI = 0.
GY = 0.	VI = 0.
CYL = -0.	ALPHA = 0.12
OMG = 1.7	NU = 0.4
	DELT = 0.02

SPECIAL BOUNDARY CONDITIONS

- i. The sliding of the top boundary is imposed by setting:

$$u_{i,j_{\max}} = 1.0; i = 1, i_{\max} - 2$$

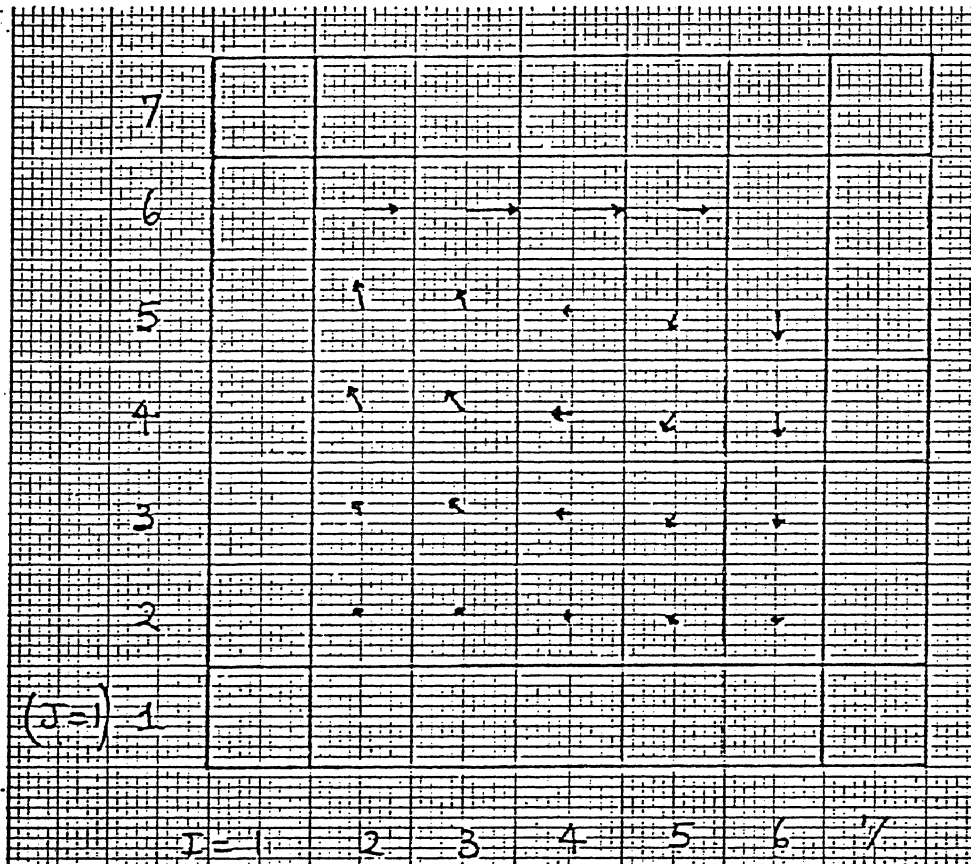


FIGURE 13. Velocity field at $t = 0.36$ for case 1:
viscous flow in a cavity

Enuma Dickson Ozokwelu
22-6 N. Univ. Pl.
Stillwater, OK 74074

July 21, 1980

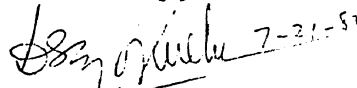
Dr. R.N. Maddox
Sheerar Professor
School of Chemical Engineering
Oklahoma State University
Stillwater, OK 74074

Dear Sir,

I wish to submit this proposal for your consideration in partial fulfillment of the requirement for my Ph.D. Qualifying Examination.

I hope it will receive your and the faculty's attention and consideration. Thanks.

Yours sincerely,



Enuma Dickson Ozokwelu

EDO/sc

"PREDICTION OF THE PERFORMANCE OF VORTEX-CONTROLLED DIFFUSER
VIA FINITE DIFFERENCE TECHNIQUE".

The vortex-controlled diffuser (VCD) employs bleed off at the throat of the diffuser to accomplish low pressure loss diffusion in a short length. Figure 1 borrowed from reference 2 illustrates the simplest form of VCD geometry. The flow diffuses from a primary duct into a suddenly expanded secondary duct. The vortex formed by the presence of the vortex fence introduces a turbulent shear action between adjacent flow streams resulting in an increase of energy of the flow stream down the secondary duct. (see fig. 2) The VCD flow mechanism is very well explained in reference 1.

Studies in various applications of VCD started only about five years ago with the extensive work at the Cranfield Institute of Technology, England. R.C. Adkins⁽¹⁾ et al, working with both tubular and annular diffuser models recommended that the new concept be used to replace existing gas turbine engine diffusers. His results showed that pressure recoveries in excess of eighty per cent may be recovered over wide range of area-ratios, with diffuser lengths of about only one-third that required by current design techniques. Only about five percent bleed off of the main air flow from the diffuser throat is required and this bleed off can be used for turbine cooling purposes. Adkins et al⁽²⁾ showed that the VCD can not only be used as a precombustor diffuser, but also can be slightly modified for use in control of exhaust gas emissions from a gas turbine engine. Following the extensive laboratory scale studies at Cranfield, the aerodynamic performance of the VCD as applied to a realistic gas turbine combustor flow path with realistic gas-turbine-diffuser inlet conditions, was studied at DDA (Detroit Diesel Allison, Division of General Motors) under AFAPL (Air Force Aero Propulsion Laboratory) sponsorship. The results proved that the VCD is applicable to gas turbine

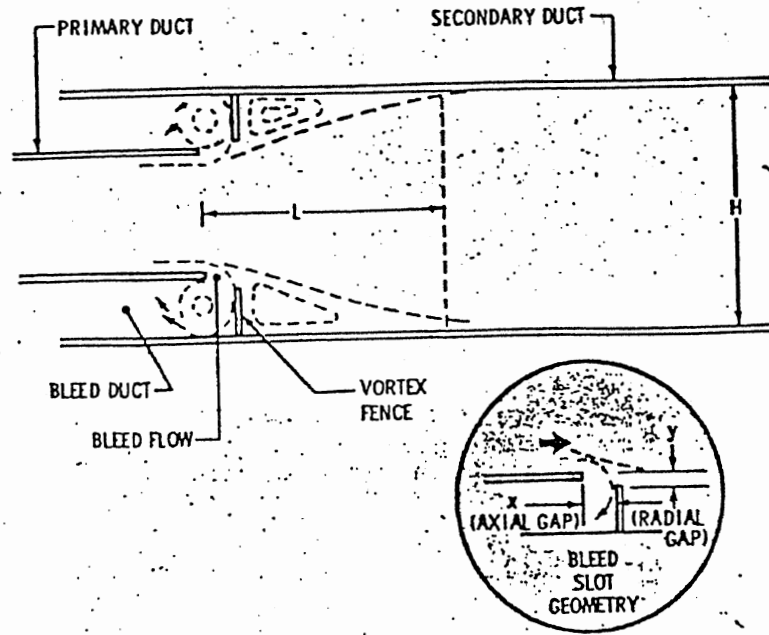
combustion systems and offers significant diffuser pressure loss reduction. The first phase of the DDA program involved experimentally obtaining the VCD component parametric performance, for use in the design of the VCD for the combustion system performance evaluation. This was necessary because, "Analytical means to predict performance with sufficient accuracy were not available for VCD performance assessment", according to reference 2.

It is therefore hereby proposed to use finite difference technique to predict the VCD component parametric performance. When accomplished, it is hoped that this approach may be more economical both money and timewise when compared with the experimental approach at the DDA. This approach would therefore be used in future to obtain VCD component parametric performance before any preliminary design is embarked upon.

According to White⁽⁵⁾, numerical techniques have proved to be the best way to obtain solutions for a number of fluid flow problems that do not have analytical solutions, more especially with the advent of large-scale digital computers. The basic equations to be solved here are the equation of continuity and the two Navier-stokes equations of motion, in both cartesian and cylindrical (axisymmetric) co-ordinates. The solution set in three dependent variables, pressure, horizontal and vertical velocities (P,U,V) of these equations will be used to compute the VCD component parametric performance. The VCD performance depends on several variables namely:

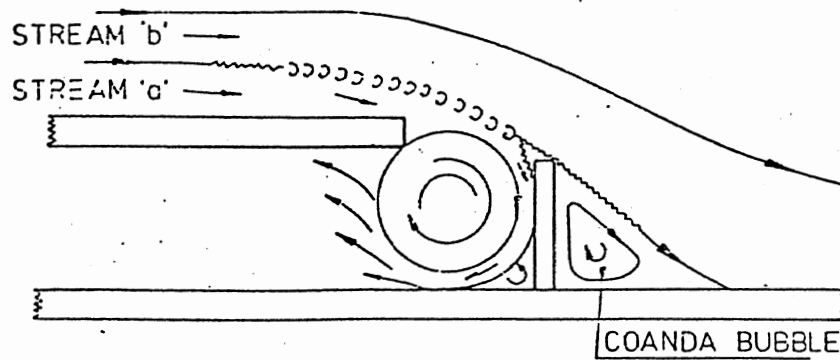
- * Secondary duct length
- * Bleed-off quantity
- * VCD area ratio (A_R)
- * VCD inlet flow distortion
- * Bleed slot radial gaps

In the final analysis, this work would be expected to come up with how the VCD performance is affected by changes in the above variables and where possible, the optimum design variables.



VORTEX-CONTROLLED DIFFUSER (VCD) GEOMETRY

FIG. 1



FLOW MECHANISM OF VORTEX CONTROL

FIG. 2

REFERENCES

1. Adkins R.C., "A short Diffuser with low pressure loss", Cranefield Institute of Technology, England, Paper presented at ASME-CSME Fluids Engineering Conference, Quebec, Canada, May 1974.
2. A.J. Verdouw, "Performance of the Vortex-controlled Diffuser (VCD) in an annular Combustor Flowpath"., Detroit Diesel Allison, Indianapolis, Indiana.
3. Adkins R.C., and Elsaflany A.S., "A double Acting Variable Geometry Combustor", Contributed by the Gas Turbine Division of the ASME for presentation at the Gas Turbine Conference and Exhibit and Solar Energy Conference, San Diego, California, March 12-15, 1979.
4. Nahavandi A.N., Holder G.D. and Borhani M.A., "Numerical Modelling of Thermal Effects in Turbulent Mixing of Large Flows"., Dept. of Chemical Engineering, Columbia Univ., N.Y., The Canadian Journal of Chemical Engineering, Vol. 57, August 1979.
5. Frank M. White, "Viscous Fluid Flow," McGraw Hill Book Company, 1974.

APPENDIX E : 1
RESULTS FROM REF. 2

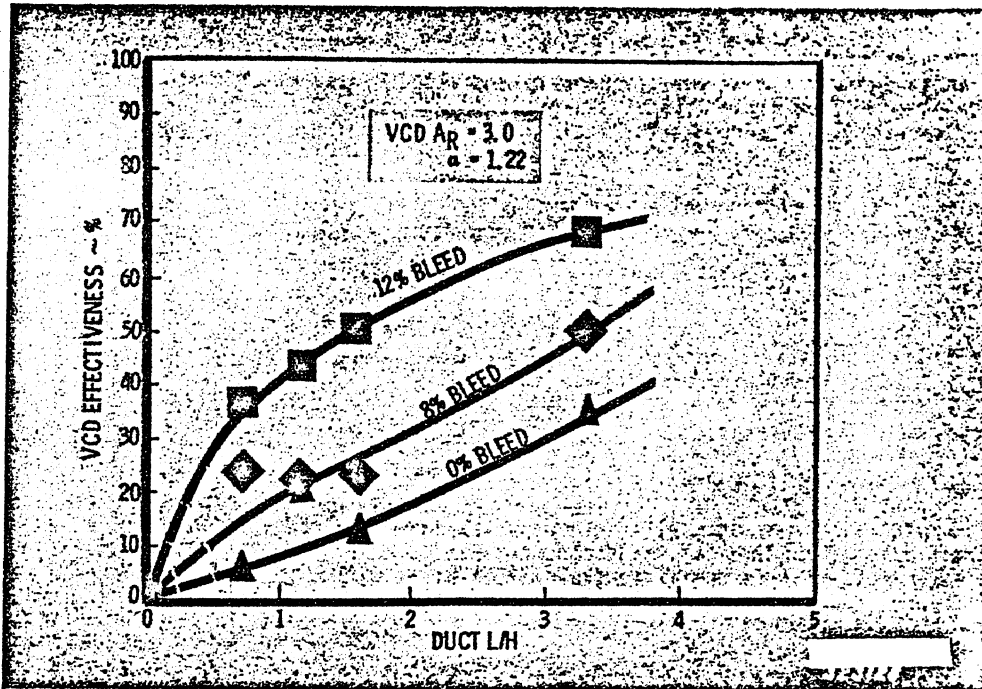


Figure 6. VCD Performance ($A_R = 3.0$)

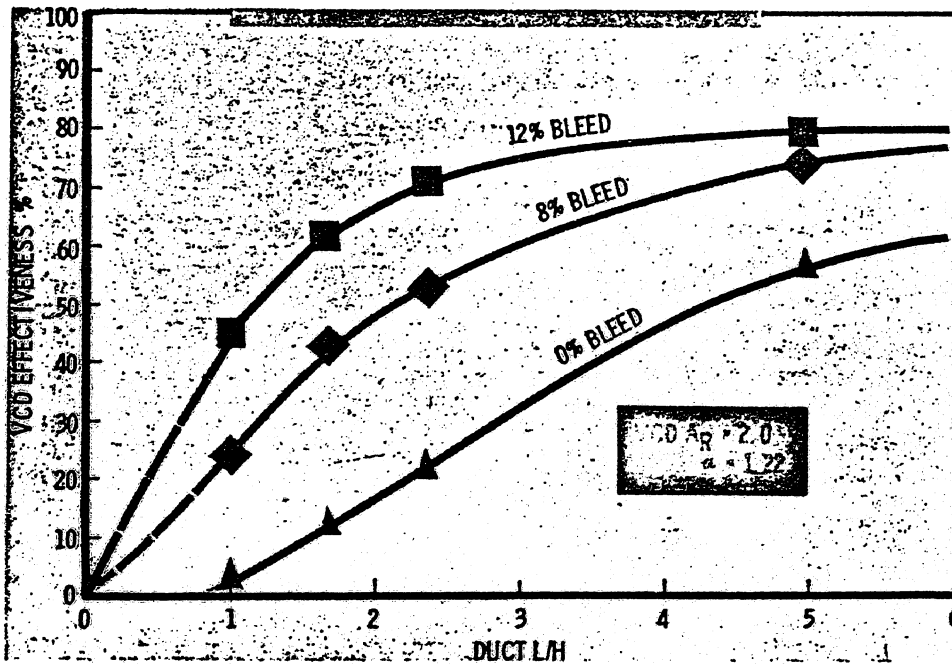


Figure 7. VCD Performance ($A_R = 2.0$)

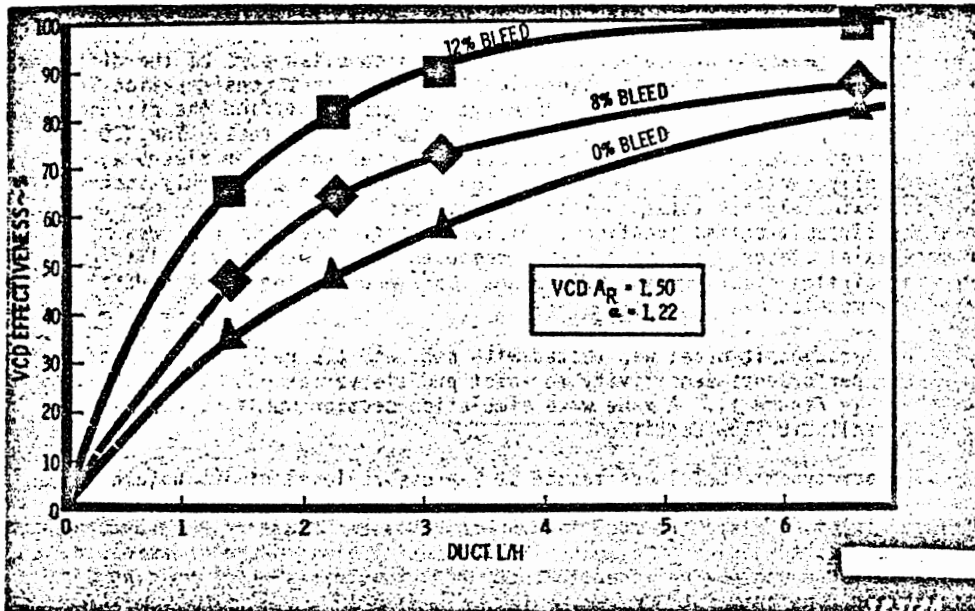


Figure 8. VCD Performance ($A_R = 1.5$)

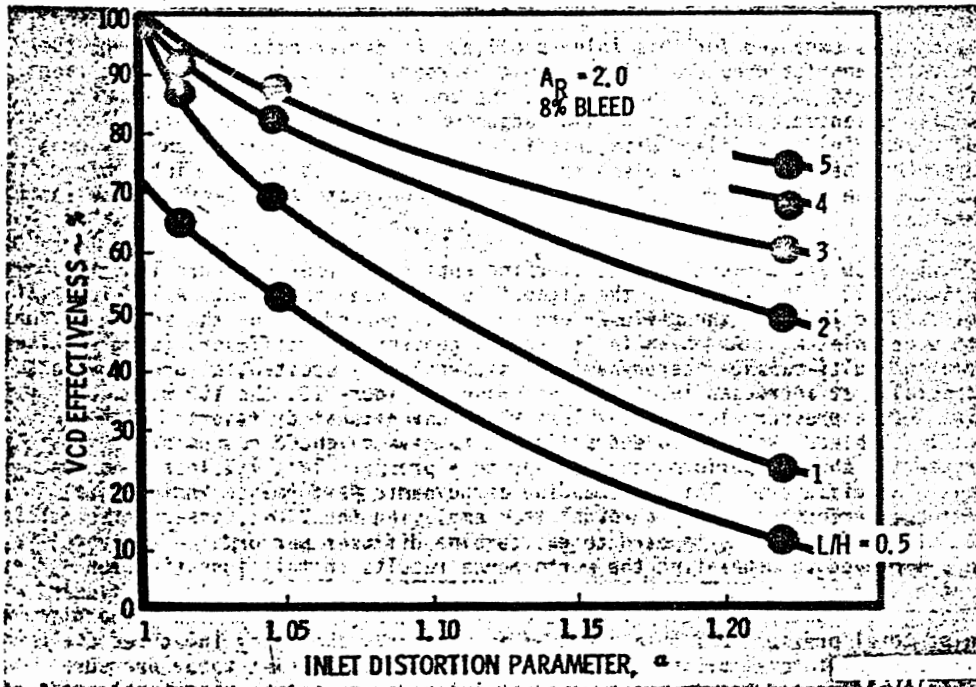


Figure 9. Effect of Inlet Distortion on VCD Performance

RESULTS FROM REF. 1.

VORTEX CONTROLLED DIFFUSER

PREDICTED COEFFICIENT OF STATIC PRESSURE RISE, C_p FOR THREE DIFFERENT INLET VELOCITY PROFILES

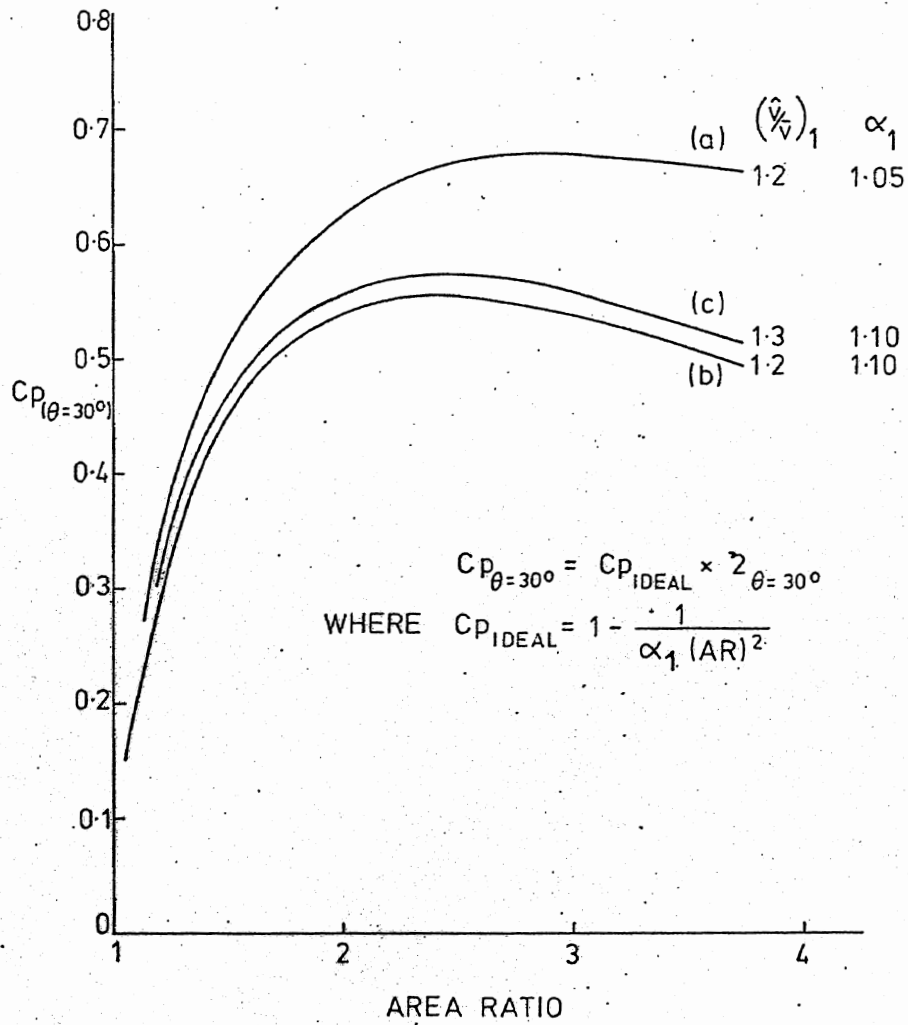


FIG. 10.